Chapter 4

Micromechanical Analysis of Polymer Fiber Composites under Tensile Loading by Finite Element Method

Ezgi Günay

Additional information is available at the end of the chapter

http://dx.doi.org/10.5772/65002

Abstract

In this chapter, the critical stress transfer factors of interface material have been studied under tensile loading. The polypropylene (PP) short fiber was embedded into the polypropylene co-ethylene (PPE) cylindrical interface first and then into the matrix material. Modified interface PPE material with lower elastic constant value than matrix material was used in our study. In this chapter, interface parameters affecting the stress transfer mechanism have been investigated. Finite element analysis (FEA) package (Ansys) has been used in the numerical modeling by using representative volume element (RVE). Tensile load was applied on one side of the composite cylinder as the other side of the composite is fixed. The critical stress-strain distributions are determined and presented by curves and tables for different fiber and interface diameters. For verification, the equivalent elastic material constants have been compared with the analytical solution and the results have been appropriate.

Keywords: FEA, representative volume element, fiber composite, stress transfer, interface, polymer

1. Introduction

There was considerable work on the determination of equivalent elastic constants of fiber-reinforced composites in the literature survey. The methods used in these studies can be summarized as follows: (i) numerical methods: finite difference and finite element method; (ii) analytical methods: semi-empirical Halpin-Tsai equation, rule of mixtures (ROM); and (iii) experimental studies in macro-, micro-, and nanoscales.

In the literature survey, studies proposing finite difference modeling and equivalent elastic properties of fiber composite structures were calculated in the consideration of the effect of fiber modulus E_f and aspect ratio (l/d) [1–6]. These studies were performed on the representative models according to both the multiple and single-fiber-reinforced material compositions.

Finite element method (FEM) is one of the most useful numerical methods in engineering problem-solving. Other methods such as the sublevel numerical procedures were additionally developed and used with FEM in solution phases. One of the main methods used was representative volume element (RVE) that used to predict the mechanical properties of unidirectional fiber composites. By using finite element analysis of RVE, effective elastic modulii of the composite were determined [7]. Experimental studies were also performed to support the numerical results [8]. Two-dimensional (unit cell method) and three-dimensional finite element analysis (FEA) with RVE was performed, and results were compared with the results of experimental studies in the literature [9–23]. Researchers often used the following FE commercial codes: ABAQUS [11, 12, 16, 19], ANSYS [17, 20], NASTRAN [13], and ALGOR-FEAS [9]. The numerically obtained results were compared and discussed with the analytical [2, 5, 14, 15, 21, 23] and experimental data in the literature survey [10, 14, 15, 18].

The aim of this study was to determine the stress and strain distributions in fiber, matrix, and fiber-matrix-interface in discontinuous fiber-matrix composite by using FEA. Each of the FE model consists of a polypropylene co-ethylene (PPE) matrix which contains a polypropylene fiber (PP) in it. In this study, 18 models were used and nine of them had also an interface volume. In this research, following six main concepts were presented by examining the single short fiber cylindrical bar within the matrix material under tensile loading for mechanical response.

1. By using RVE, testing the effectiveness of the finite element modeling procedures on the results, that is, mesh element types, meshing, definition and implementation of the boundary conditions, application of the tensile loading.
2. Considering the different volume fractions, testing the effectiveness of the various volume fraction of the fiber on the stress transfer mechanism from matrix to fiber material.
3. In terms of three-dimensional analysis, to investigate the influence of definition and modeling of interface volume between fiber and matrix in 3D.
4. In terms of three-dimensional analysis, examining the effects of fiber surface area on the stress transfer mechanism.
5. Establishing the explanations and curves for clarification the stress and strain localization at the ends of the fiber.
6. Calculating the equivalent elastic constant E_1.

http://dx.doi.org/10.5772/65002

2. The fiber-reinforced composite material with interface volume: modeling by representative volume element (RVE) method

Cylindrical RVE was used to represent the matrix and fiber all together. The different material properties of fiber, matrix, and interface were selected. The elastic constants of the polymer material were expressed as $E_m = 1.05$ GPa, $\nu_m = 0.33$, $E_f = 4.5$ GPa, $\nu_f = 0.2$, $E_i = 0.1 \times E_m = 0.105$ GPa [4], $\nu_i = 0.33$. Here, E_m, ν_m, E_f, ν_f, E_i, ν_i reflected the Young's modulus and Poisson's ratio of the matrix, fiber, and interface materials, respectively. While the fiber material was composed of elastic polyethylene (PE), the matrix and interface materials were composed of bilinear material (PPE). The thickness t_i of the interface region was defined as $t_i = 0.025d$. Here, d was the diameter of the fiber. The shear modulus of the interface region was defined as $G_i = 0.1\ G_m$ [4]. In 3D composite modeling steps, nine different geometrical properties were used with variable thickness t_i, diameter d_i, and fiber volume fraction V_f as shown in **Table 1**. According to these different geometric values, fiber composite RVE was modeled by FEM and the stress-strain transmission conditions from fiber to interface and stress transfer from interface to matrix of the three types of materials were examined.

Fiber interface thickness $t_i(\mu\text{m})$	**Fiber diameter** d (μm)	**Fiber volume fraction** V_f (%)	**Rule of mixtures (L = ℓ),** E_1 (GPa)
1	40	4.98	1.222
1.125	45	5.87	1.283
1.25	50	6.75	1.283
1.375	55	7.63	1.313
1.5	60	8.51	1.344
1.625	65	9.37	1.373
1.75	70	10.22	1.403
1.875	75	11.06	1.432
2	80	11.87	1.459

Table 1. PPE/PP single-fiber-matrix modeling according to the various interface geometric properties and analytical results of continuous $(L = \ell)$ fiber-matrix composite.

Fiber volume fraction values and the size of the material models were obtained by using the following equation [13];

$$V_f = \frac{\pi \ell d^2}{4LS^2} \tag{1}$$

Here, ℓ, L, and S correspond to the fiber spacing, fiber length, and longitudinal fiber spacing, respectively, as shown in **Figure 1**.

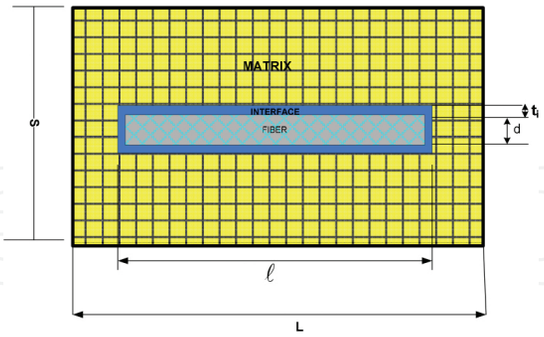

Figure 1. 2D geometrical parameters of the matrix/interface/fiber combination of PPE/PP microcomposite.

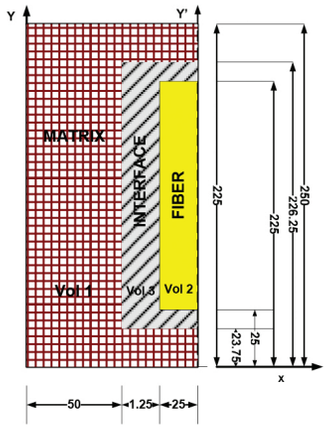

Figure 2. One of the typical geometrical descriptions of the polymer composite (matrix/interface/fiber, d = 50 μm) and generated volume numbers.

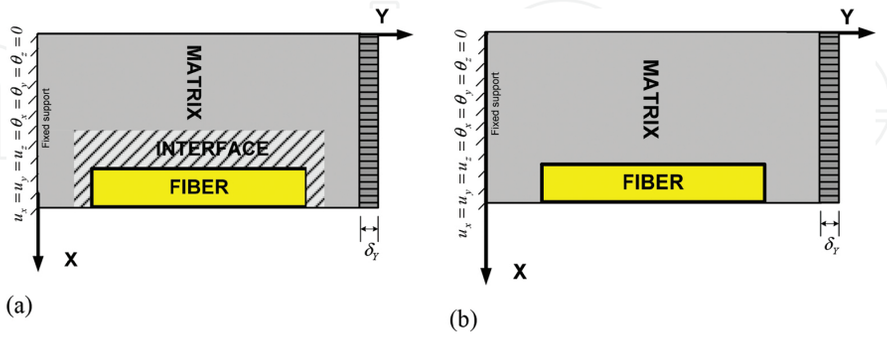

Figure 3. Two different RVE fiber composite geometries and applied displacement boundary conditions: (a) fiber, interface, and matrix combination; (b) fiber and matrix combination.

By rotating the 2D model 360° around the Y'-axis, 3D material models were obtained as shown in **Figure 2**. Cylindrical geometry was divided into two segments and one segment was

http://dx.doi.org/10.5772/65002

used to demonstrate the results (**Figures 2** and **3**). In general, the cylindrical geometry was defined in cylindrical coordinates (r, θ, z). In Ansys, modeling (x, y, z) Cartesian coordinate axes refers to the (r, θ, z) in the cylindrical coordinate system. However, in this study, all of the results and Ansys code screen outputs were demonstrated only on the *x-y* plane of the projected surface for one half of the cylindrical geometry.

2.1. Analytical formulation.

The aim of the micromechanical approaches was to determine the equivalent elastic constants of composite material considering individual elastic constants constituting the composite material. The equivalent elastic constants $\left(E_1,\ E_2, G_{12}, \nu_{12}\right)$ of the fiber-reinforced-composite have been determined analytically in terms of the relative volume fractions $\left(V_f,\ V_m\right)$ and elastic constants $\left(E_f,\ E_m, G_f, G_m, \nu_f, \nu_m\right)$ of fiber and matrix. It may be mentioned two basic analytical approaches in micromechanics of continuous fiber-matrix composite materials in obtaining the equivalent elastic constants. The first one was the rule of mixtures (ROM), and the second one was the Halpin-Tsai semi-empirical model [24, 25]. The first model "rule of mixtures" defined as the mathematical expressions that give the elastic properties of the continuous fiber composite material in terms of original material properties, volume fiber fraction, and arrangement of its constituents: (a) the apparent Young's modulus in the same direction as the fibers (E_1) (Eq. (2)), (b) the apparent Young's modulus in the direction perpendicular to the fibers (E_2) (Eq. (3)), (c) the major Poisson's ratio (ν_{12}) (Eq. (4)), and (d) the in-plane shear modulus (G_{12}) of a lamina (Eq. (5)). Rule of mixtures (ROM) equations have been listed and shown as the formulas below:

$$E_1 = E_f V_f + E_m\left(1 - V_f\right) \tag{2}$$

$$E_2 = \frac{E_f E_m}{V_m E_f + V_f E_m} \tag{3}$$

$$\nu_{12} = V_f \nu_f + \nu_m\left(1 - V_f\right) \tag{4}$$

$$G_{12} = \frac{G_m G_f}{V_m G_f + V_f G_m} \tag{5}$$

The second model "Halpin-Tsai" included the expressions obtained by curve fitting as: (a) the apparent Young's modulus in the same direction as the fibers (E_1) (Eq. (6)), (b) the apparent

Young's modulus in the direction perpendicular to the fibers (E_2) (Eq. (7)), (c) the major Poisson's ratio (ν_{12}) (Eq. (8)), and (d) the in-plane shear modulus (G_{12}) (Eq. (9)) of a single layer of layered composite "ply." These related equations have been listed and shown below:

$$E_1 = E_f V_f + E_m V_m \tag{6}$$

$$\frac{E_2}{E_m} = \left[\frac{1+\xi\eta V_f}{1-\eta V_f}\right] \quad \eta = \frac{\left[\frac{E_f}{E_m}\right]-1}{\left[\frac{E_f}{E_m}\right]+\xi} \tag{7}$$

$$\nu_{12} = V_f \nu_f + \nu_m V_m \tag{8}$$

$$\frac{G_{12}}{G_m} = \frac{1+\xi\eta V_f}{1-\eta V_f} \quad \eta = \frac{\left[\frac{G_f}{G_m}\right]-1}{\left[\frac{G_f}{G_m}\right]+\xi} \tag{9}$$

The reinforcing factor (ξ), measuring reinforcement of the composite, is variable depending on the fiber geometry, packing geometry, and loading condition. It is a measure of reinforcement of the composite. The values of ξ have been obtained by comparing the Eqs. (7) and (8) with exact elasticity solutions, and corresponding curve fitting results. The generalized Hooke's law equation is as follows:

$$\sigma_i = C_{ij}\varepsilon_j \tag{10}$$

In this equation, σ_i is the stress vector, C_{ij} is the stiffness matrix, and ε_i is the strain vector components. In functional form, C_{ij} has been represented by Eq. (11) in terms of the elastic properties of the fiber, matrix, relative volume fractions of fiber and matrix.

$$C_{ij} = C_{ij}\left(E_f, \nu_f, V_f, E_m, \nu_m, V_m\right) \tag{11}$$

In most literature studies, the basic analytical approaches have been presented without taking into account the adhesion of the interface across the end faces of the fibers and the stress concentration effects at the fiber ends [2, 26, 27].

http://dx.doi.org/10.5772/65002

3. Finite element modeling of short fiber in microcomposite and analyses results

In the literature survey, a detailed examination on fiber-reinforced polymer matrix composites was observed in determining the most suitable fiber-matrix combination model. In the literature, different studies were found about tension/compression and shear loading to the different modeling types of fiber/interface/matrix combinations, and in these studies, the strength of the applied tensile/compression and shear loading types have been investigated. In this research, the stress transfer mechanism and equivalent elastic constants of short fiber composites were tried to be obtained by using new modeling. In FE modeling, the design criteria were as follows: the dimensions of fiber and matrix, the material types of fiber and matrix, the dimensions and material types of interface volume and the application of the tensile load. In the first stage of the study, a single short fiber was studied with ANSYS code in determining the optimum interface thickness by comparing the results obtained. In this step, two different models were tested. The first one was fiber-matrix microcomposite with interface (**Figure 3a**); the second model was fiber-matrix microcomposite without interface (**Figure 3b**). In the second stage of the study, the effects of interface volumes on the values of stress distributions around the tip points of the fiber were attempted to explain. In the calculation of the single-fiber modeling, nine different interface thicknesses t_i and nine different fiber diameters d_i were used $t_i = 0.025\ d_i$, ($d_i = 40, 45, ..., 80\ \mu$m). In this study, the interface volume was defined around all of the faces of the fiber. In the literature, the studies were performed by defining the interface surface or volume along the longitudinal surface (**Figure 3**).

Fiber diameter d (μm)	**Number of mesh elements and nodes in the fiber-interface-matrix model (SHELL93)**	**Elastic constant** E_1 (GPa) **(fiber-interface-matrix model)**	**Number of mesh elements and nodes in the fiber-matrix model (SHELL93)**	**Elastic constant** E_1 (GPa) **(fiber-matrix model)**
40	31,776/93,823	1.472	2271/6680	1.054
45	16,520/48,859	1.465	2475/7238	1.056
50	11,503/33,926	1.459	2474/7237	1.057
55	33,190/98,585	1.449	2543/7438	1.081
60	33,155/98,478	1.446	2559/7486	1.063
65	21,104/62,686	1.415	2957/8668	1.066
70	14,298/42,267	1.428	2998/8795	1.065
75	15,029/44,458	1.441	3103/9110	1.035
80	15,604/46,171	1.411	3229/9480	1.047

Table 2. The used geometric parameters, mesh elements, node numbers, and obtained elastic constants of discontinuous $(L\rangle\ell)$ fiber-matrix microcomposite.

In this study, the short single-fiber composite polymer (PPE/PP) material was modeled in microlevel by finite element method (FEM). Single-fiber arrangement in matrix under the axial loading was adequate to explain the overall characteristics of the fiber composite structures. SHELL93 as ANSYS element type was used. This element has 6 degree of freedom per node $\left(u_x, u_y, u_z, \theta_x, \theta_y, \theta_z\right)$. The generated FE models for nine different geometries have different total number of mesh elements and node numbers. Exact number of elements and nodes corresponding to the composite models has been summarized in **Table 2**.

Composite model consists of three volume sections representing the fiber matrix and interface (**Figure 4**). The first boundary condition of the model was applied by fixing one end of the geometry, and this was performed by setting the 6 degree of freedom of each node to zero (BC_1).

The second boundary condition of the model was related with the loading condition. The second end of the composite cylinder was pulled with a constant load. The loading magnitude applied to the nodes was $P = 0.1$ N. In this application, because of the unsymmetrical meshing system, the resultant deformation of the bar was obtained as unsymmetrical. In order to overcome this difficulty, second boundary condition was applied to the second end of the cylinder. On this face along the loading application thickness or level $\left(t_{app}\right)$, the "unit displacement" $U_y = 0.1\ \mu$m was adopted to each node to obtain the symmetric displacement condition over the whole body $\left(1\ \mu\text{m} \le t_{app} \le 2\ \mu\text{m}\right)$ (BC_2) (**Figure 3**). The stress concentration regions were developed between the fiber and matrix at the sharp edge corners as shown in **Figures 5–8**. Fiber-matrix model showed higher stress concentrations than fiber-matrix-interface model. In order to give more explanation to the developing stress distributions on these faces, the third boundary condition was applied (BC_3). The previously defined first- and second-type boundary conditions were applied over the extremely large sections of the body $\left(20\ \mu\text{m} \le t_{app} \le 26\ \mu\text{m}\right)$, and new stress distribution results were obtained (**Figures 9** and **10**).

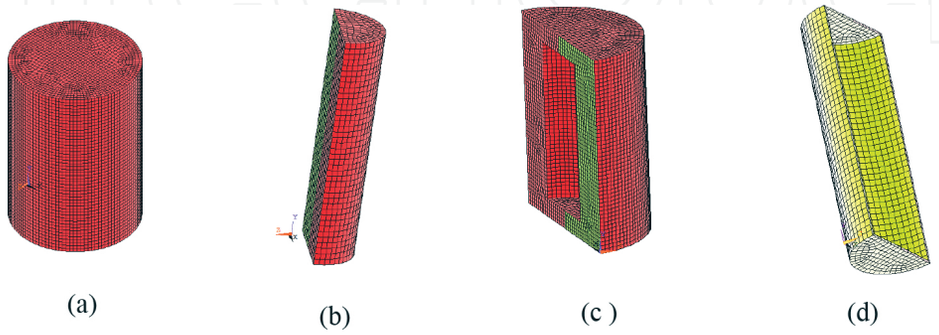

Figure 4. FEA meshing with SHELL93 element (a) RVE of fiber cylindrical composite model, (b) fiber, (c) matrix, and (d) interface.

http://dx.doi.org/10.5772/65002

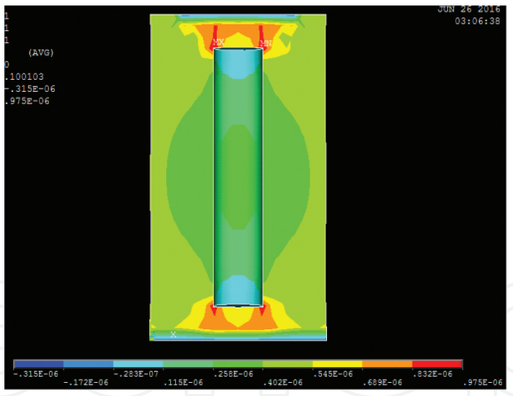

Figure 5. Stress (σ_y) distribution on the matrix section obtained from FEA nodal solution without interface region ($d = 40\ \mu$m).

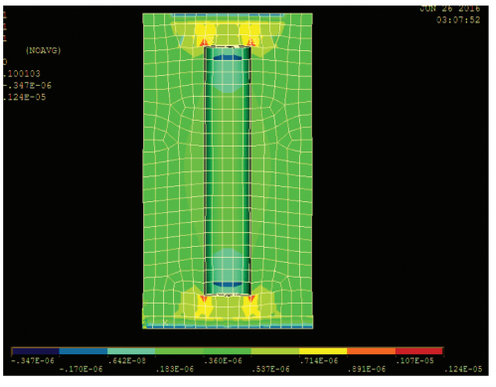

Figure 6. Stress (σ_y) distribution on the matrix section obtained from FEA element solution without interface region ($d = 40\ \mu$m).

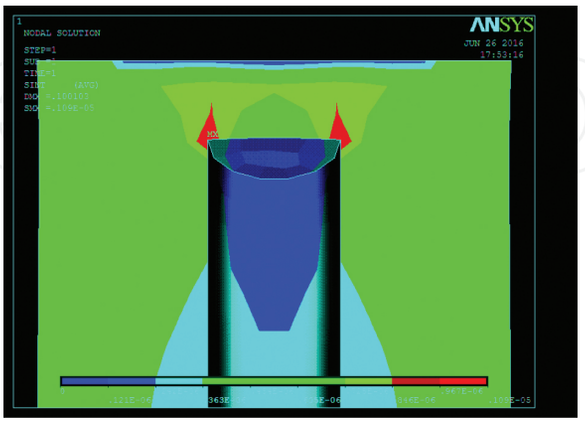

Figure 7. Stress (σ_y) intensity on the matrix section obtained from FEA element solution without interface region ($d = 40\ \mu$m).

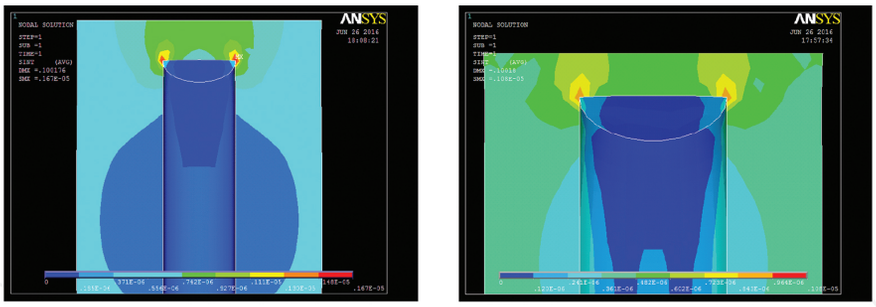

(a) (b)

Figure 8. Stress (σ_y) intensity developing on the matrix section (a) with interface region, (b) without interface region ($d = 80\ \mu$m).

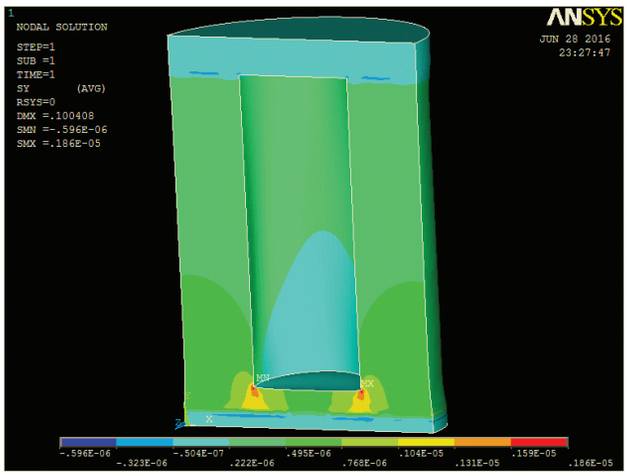

Figure 9. FE results for the BC_2, $\left(\sigma_y\right)$ stress localization which is parallel to the applied displacement loading δ_y and generated around the sharp corners of the fiber–matrix model without interface region ($d = 80\ \mu$m).

Figures 5–7 have been represented the σ_y distribution developing within the composite model in matrix segment with noninterface case for the fiber diameter $d = 40\ \mu$m [2]. The stress distributions were defined for both nodal and elemental solutions. The developing stress localizations appeared around the tip sections of the fiber in matrix. The developing maximum stress distributions were intensified around the fiber end sections. At the same region around the neighborhood sections of the fiber segment, stress levels reached to relatively lower stress localizations in comparison with maximum. This stress distribution was wide spread around the maximum stress localization in a definite region. Normal stress value reached to their secondarily largest value around the middle section of the fiber in matrix material. Additionally, nodal solution curves gave better results than elemental solution. In nodal solution, stress localizations appeared in a narrower region with longer segments. In finite element analysis, element solutions were obtained by Gauss quadrature integration points. Nodal solution results were determined at the coordinates of the nodal points by interpolation functions.

http://dx.doi.org/10.5772/65002

Gauss integration points have been defined at the inner section of the elements which were not coincided with nodal coordinates. These element solutions were obtained by using the interpolating functions in the curvilinear coordinate system. Element types varied according to the interpolation functions used. In the generated composite models, the generated total number of elements, nodes, and the obtained results were listed in **Table 2**. When the number of elements increased, the most correct results were obtained. For these processes, high-capacity computer systems were required. Stress distributions developing on the fiber and matrix sections without interface volume were presented in **Figures 11** and **12**. In these figures, stress localizations were developed on both matrix and fiber surfaces.

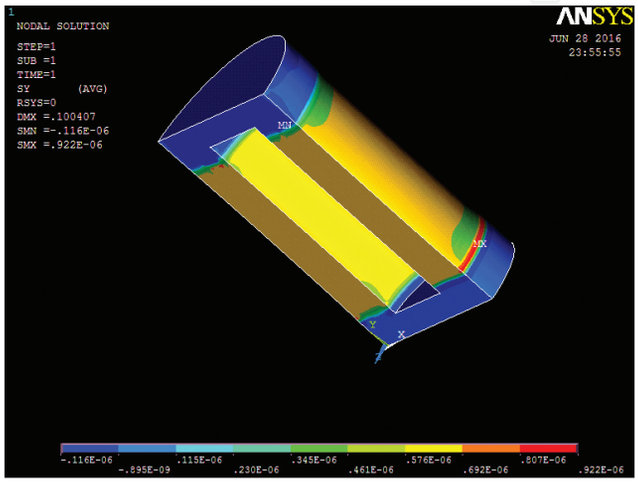

(a)

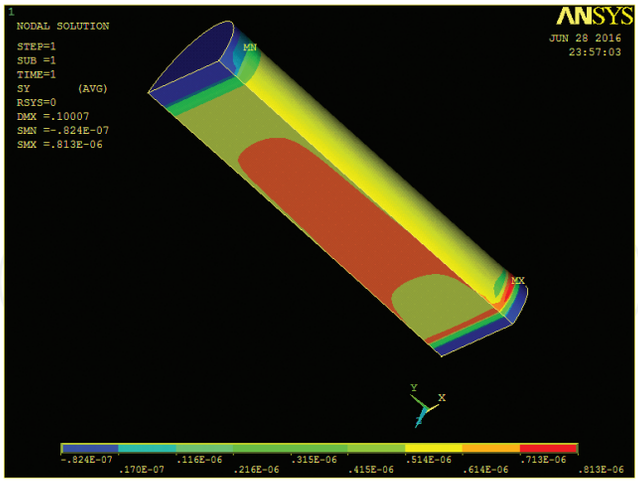

(b)

Figure 10. FE results for the BC_3, $\left(\sigma_y\right)$ stress localization on the (a) matrix and (b) fiber which are parallel to the applied displacement loading δ_y and generated above the sharp corners of the fiber–matrix model without interface region ($d = 75\mu m$).

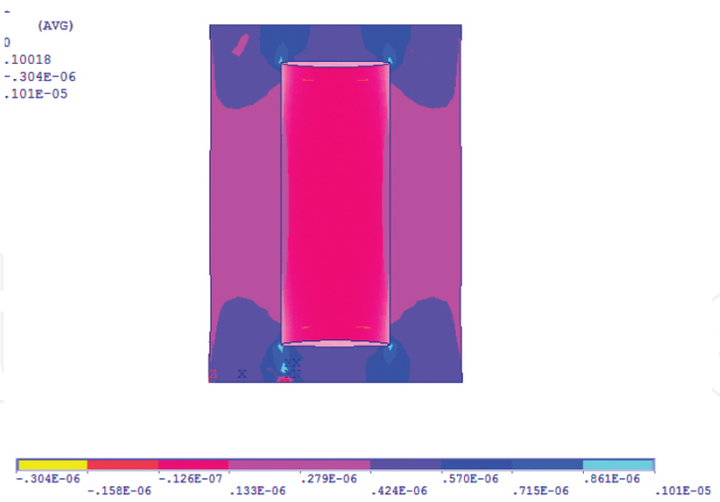

Figure 11. FEA stress $\left(\sigma_y\right)$ distribution developing on the matrix section of the fiber-matrix model without interface region ($d = 80\ \mu$m).

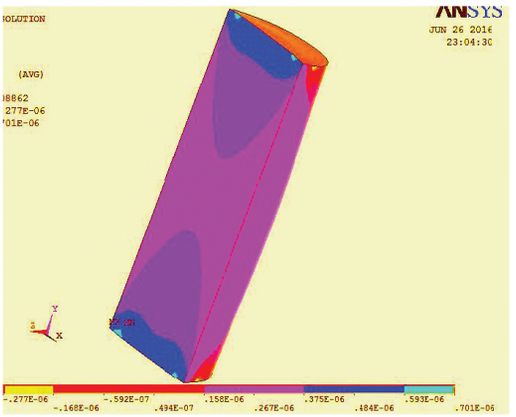

Figure 12. Stress (σ_y) distribution on the fiber section obtained from the FEA without interface region ($d = 80\ \mu$m).

As the fiber diameter decreased, the stress distributions collected at the end surface of the cylindrical fiber material grown locally. When the stress localizations reduced in the interface region between matrix and fiber at the same time, higher stresses in fiber section has emerged. As it has shown by **Figures 13** and **14**, in the polymer fiber model with an interface region, the maximum stress value was $\sigma_y = 0.952 \times 10^{-6}\ \text{N}/\mu\text{m}^2$, and in the polymer fiber model without interface, maximum stress developing on the fiber was equal to $\sigma_y = 0.732 \times 10^{-6}\ \text{N}/\mu\text{m}^2 (d = 40\ \mu\text{m})$. On the other hand, in the model with an interface, matrix sections near to the fiber had the value $\sigma_y = 0.265 \times 10^{-6}\ \text{N}/\mu\text{m}^2$, and in the noninterface model, stress value was $\sigma_y = 0.429 \times 10^{-6}\ \text{N}/\mu\text{m}^2$ (**Figures 15** and **16**) ($d = 40\ \mu$m).

http://dx.doi.org/10.5772/65002

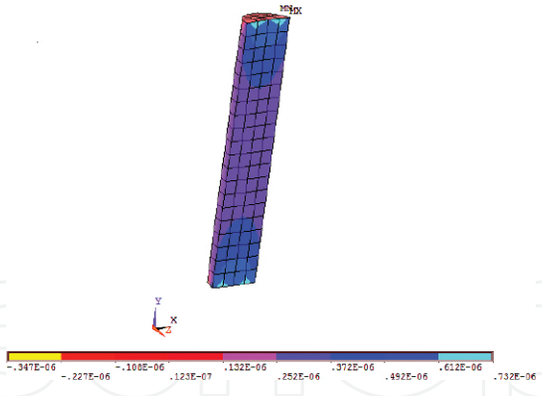

Figure 13. FEA stress $\left(\sigma_y\right)$ distribution developing on the fiber section of the fiber-matrix model without interface region ($d = 40\ \mu$m).

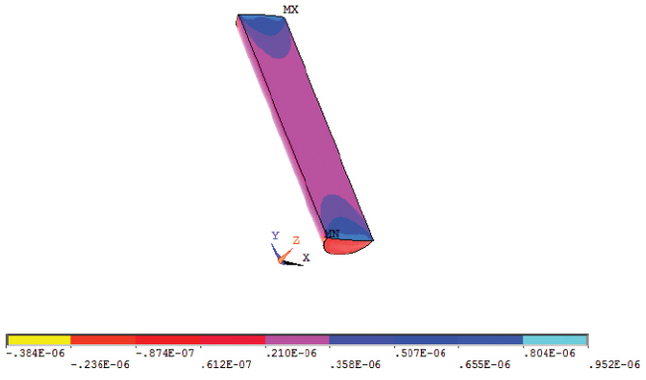

Figure 14. FEA (σ_y) distribution developing on the fiber section of the fiber-matrix model with interface region ($d = 40\ \mu$m).

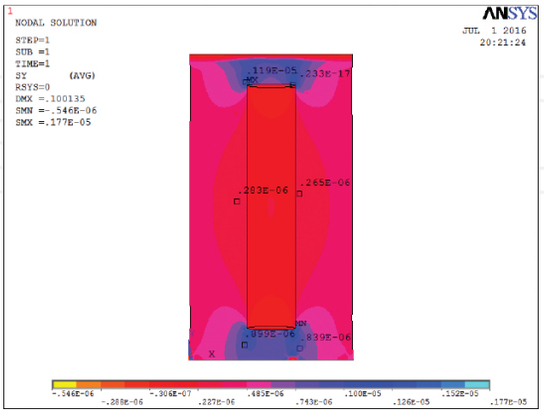

Figure 15. Stress $\left(\sigma_y\right)$ distribution developing on the matrix section of the fiber-matrix model with interface ($d = 40\ \mu$m).

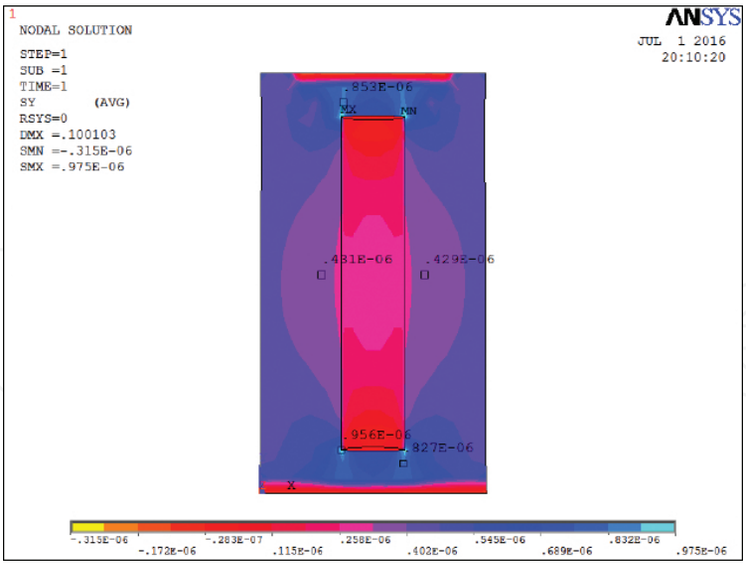

Figure 16. Stress $\left(\sigma_y\right)$ distribution developing on the matrix section of the fiber-matrix model without interface ($d = 40\ \mu$m).

When the models were analyzed in terms of interface thicknesses, in the models with thicker interface, the stress was found to be more. The interface region with the largest diameter had the largest stress σ_y and Von Mises stress σ_2 distributions relative to the smallest one. These were equal to $\sigma_y = 0.130 \times 10^{-5}\ \text{N}/\mu\text{m}^2$ (**Figure 17**) and $\sigma_2 = 0.132 \times 10^{-5}\ \text{N}/\mu\text{m}^2$ (**Figure 18**) for $d = 40\ \mu$m and $\sigma_y = 0.08967\ \text{N}/\mu\text{m}^2$ (**Figure 19**) and $\sigma_2 = 0.233 \times 10^{-5}\ \text{N}/\mu\text{m}^2$ (**Figure 20**) for $d = 80\ \mu$m. Having studied the **Figures 21** and **22**, it was seen that the maximum stress distributions are developed at the tip corner sections of the interface geometries. Nodal solution results of $\sigma_y = 0.149 \times 10^{-5}\ \text{N}/\mu\text{m}^2$ for $d = 40\ \mu$m and $\sigma_y = 0.154 \times 10^{-5}\ \text{N}/\mu\text{m}^2$ for $d = 80\ \mu$m were obtained.

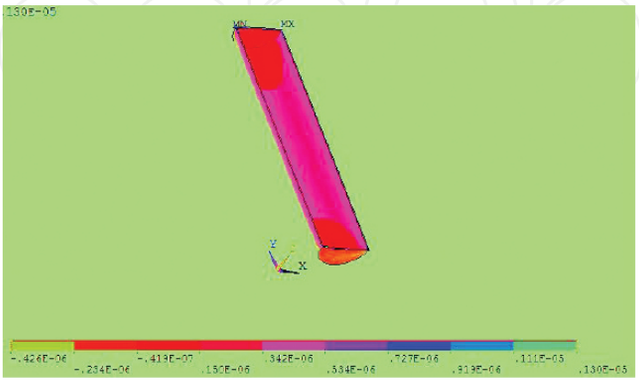

Figure 17. FEA $\left(\sigma_y\right)$ distribution developing on the interface section of the fiber–matrix model ($d = 40\ \mu$m).

http://dx.doi.org/10.5772/65002

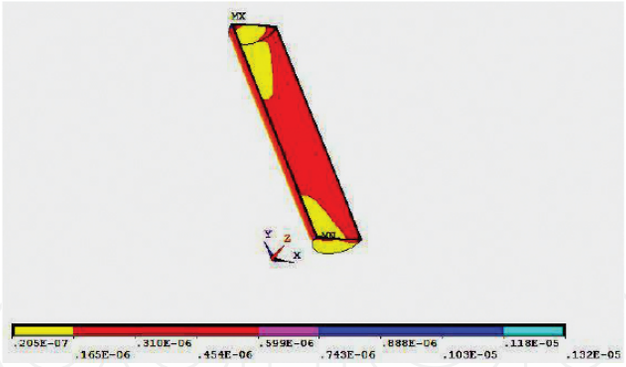

Figure 18. FEA Von Mises (σ_2) distribution developing on the interface section ($d = 40\ \mu$m).

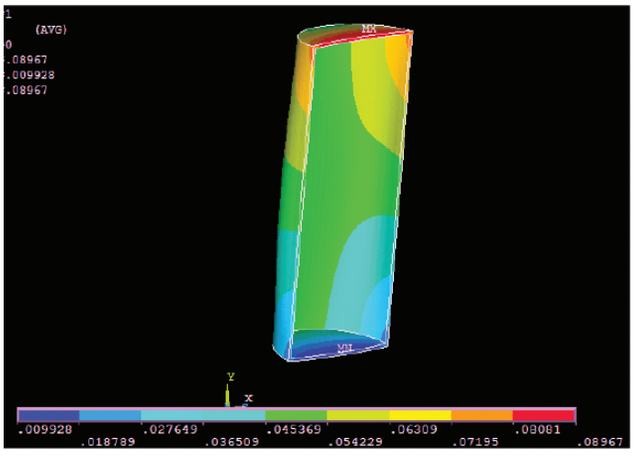

Figure 19. Stress (σ_y) distribution on the interface section obtained from FEA nodal solution ($d = 80\ \mu$m).

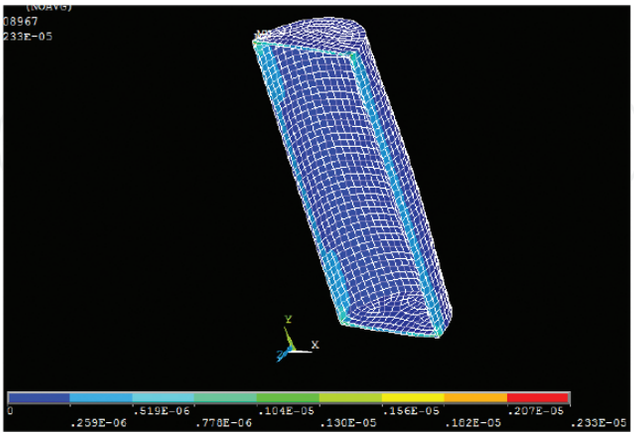

Figure 20. Von Mises (σ_2) stress distribution on the interface section obtained from FEA nodal solution ($d = 80\ \mu$m).

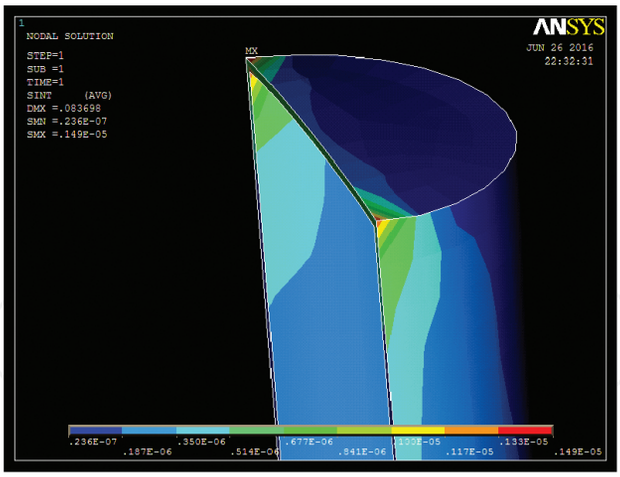

Figure 21. Stress intensity on the interface section ($d = 40\ \mu$m).

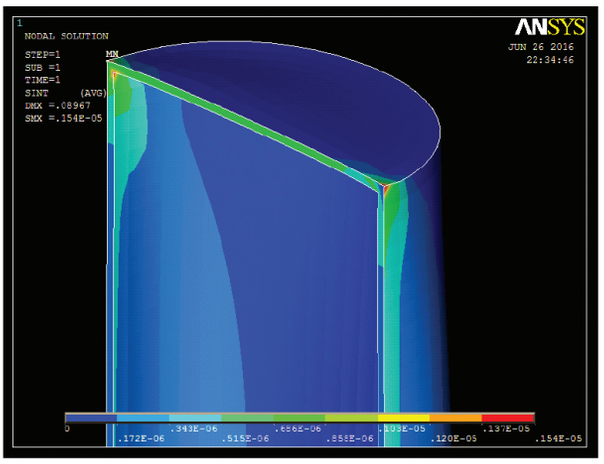

Figure 22. Stress intensity on the interface section ($d = 80\ \mu$m).

For nine different interface geometries, FEA results were represented by curves. These curves included the results for the fiber diameters between 40 and 80 μm, and corresponding thicknesses were $t_i = 0.025(40) = 1, ..., t_i = 0.025(80) = 2$ (**Table 1**). The overall stress-strain distributions developed in the composite were affected by the thicknesses of the interface region, and these were proportional to the fiber diameter. As it has shown by **Figure 23**, the largest interface stresses were developed in the models with the diameters $d = 40\ \mu$m and $d = 55\ \mu$m. As the interface grew in diameter, the interface stresses became diminished from 6.9×10^{-7} to 5.5×10^{-7} N/μm^2. **Figure 23** presents the suddenly changed stress intensity values at the tip points of the fiber. Shear stress distributions τ_{xy} and τ_{yz} along the main axis Y' (**Figure 2**) were shown with curves. In **Figures 24** and **25**, shear stresses were found to be changed suddenly around the corner sections of the fiber end portion. The largest shearing stresses in fiber-reinforced microcomposites have been developed with the largest diameters. In summary,

http://dx.doi.org/10.5772/65002

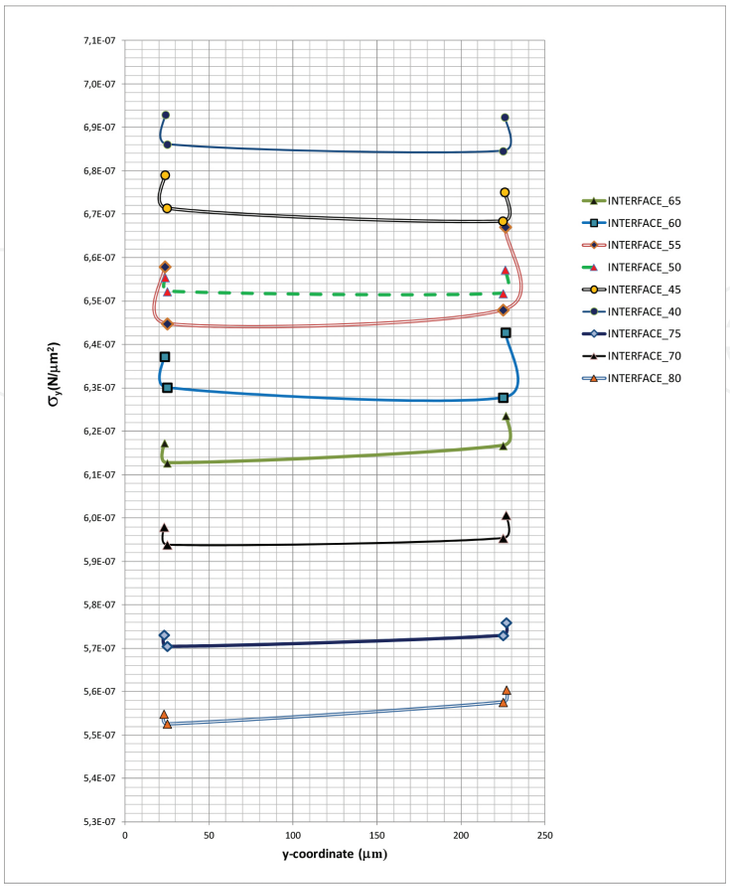

Figure 23. FEA results for σ_y stress distributions on nine different interface regions of the fiber-matrix (RVE) under tensile load.

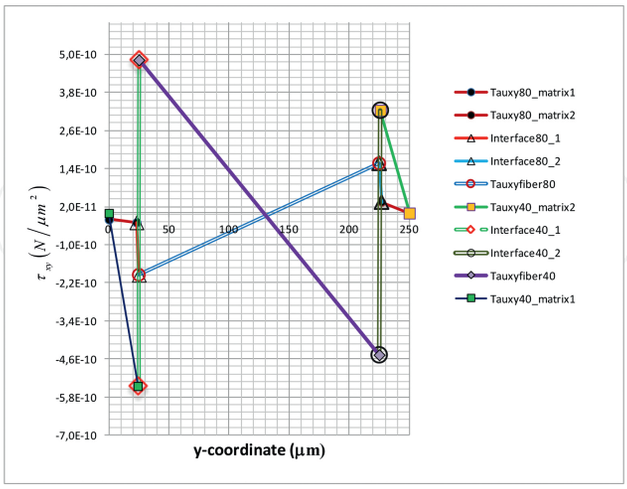

Figure 24. Comparison of stress $\left(\tau_{xy}\right)$ distributions along the main y-axis of the fiber composite in microscale for the fiber diameters $d = 40\ \mu$m and $d = 80\ \mu$m.

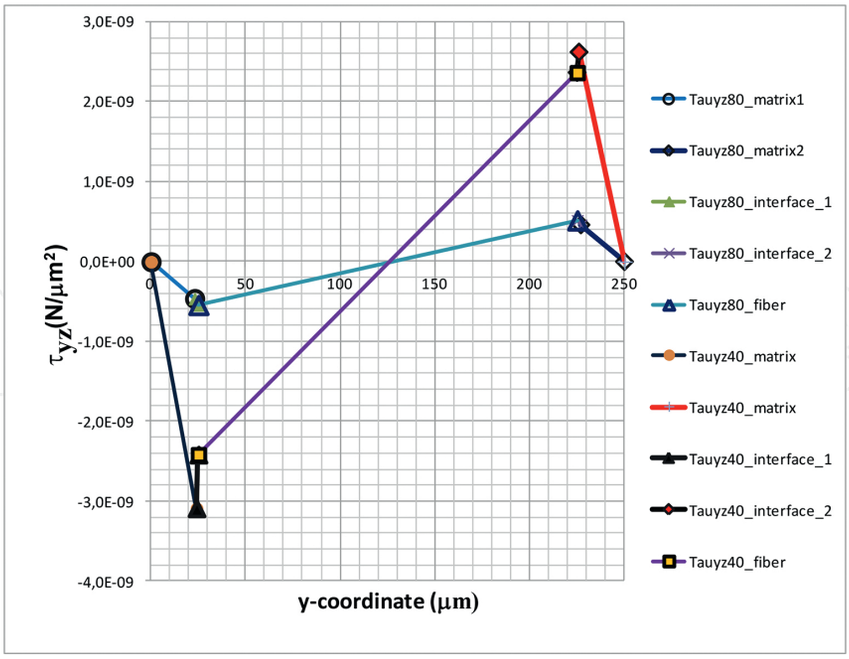

Figure 25. Comparison of stress $\left(\tau_{yz}\right)$ distributions along the main y-axis of the fiber composite in microscale for the fiber diameters $d = 40\ \mu$m and $d = 80\ \mu$m.

$$\left|\tau_{xy}\right|_{\max} = 5.8\times10^{-10}\ \text{N/}\mu\text{m}^2 \quad d = 40\ \mu\text{m} \tag{12}$$

$$\left|\tau_{xy}\right|_{\max} = 3.5\times10^{-10}\ \text{N/}\mu\text{m}^2 \quad d = 80\ \mu\text{m} \tag{13}$$

$$\left|\tau_{yz}\right|_{\max} = 3.0\times10^{-9}\ \text{N/}\mu\text{m}^2 \quad d = 40\ \mu\text{m} \tag{14}$$

$$\left|\tau_{yz}\right|_{\max} = 0.5\times10^{-9}\ \text{N/}\mu\text{m}^2 \quad d = 80\ \mu\text{m} \tag{15}$$

The stress-strain $\sigma_y - \varepsilon_y$ curves were plotted in FE models for diameters $d = 40\ \mu$m, $d = 70\ \mu$m, and $d = 80\ \mu$m. These are presented in **Figure 26**. From the slopes of these curves, the elastic constant values parallel to the fiber and loading direction $\left(E_1\right)$ were obtained and results are listed in **Table 2** for both fiber-matrix and fiber-interface-matrix models. These models have provided an opinion to the resultant data for $\left(E_1\right)$. FE model for the short fiber composite without interface case gave the value as $\left(E_1\right)_{avg} = 1.058$ GPa, and for the short fiber composite with interface case, it was $\left(E_1\right)_{avg} = 1.446$ GPa.

http://dx.doi.org/10.5772/65002

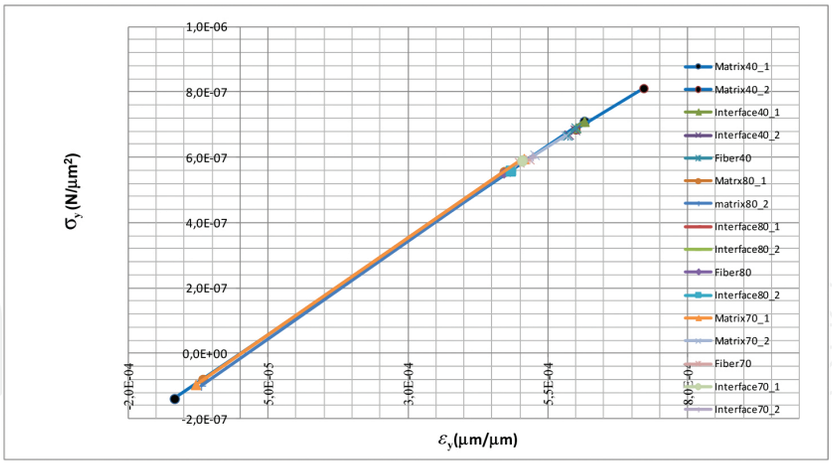

Figure 26. Stress-strain curves of FE-RVE models for fiber diameters $d = 40\ \mu$m, $d = 75\ \mu$m and $d = 80\ \mu$m.

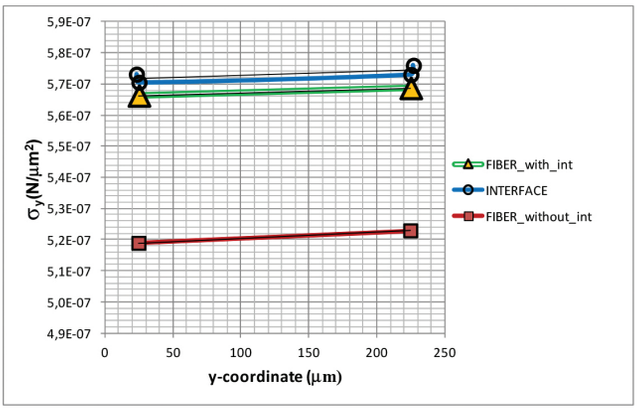

Figure 27. Comparison of stress distributions $\left(\sigma_y\right)$ obtained from the interface segment of the RVE-FE model ($d = 75\ \mu$m): (a) fiber with interface, (b) interface, (c) fiber without interface.

Figure 27 presented the comparison of σ_y distribution for (a) fiber without interface, (b) interface, and (c) fiber with interface regions. As it has shown in the curve for $d = 75\ \mu$m, fiber with interface and also interface region stresses were near to each other in magnitudes $5.7 \times 10^{-7}\ \text{N}/\mu\text{m}^2$. In case, fiber without interface showed the σ_y distribution around $5.2 \times 10^{-7}\ \text{N}/\mu\text{m}^2$. The difference between them was equal to $0.5 \times 10^{-7}\ \text{N}/\mu\text{m}^2$.

4. Discussion and conclusion

The effectiveness of the imposed interface volume and its geometric properties on the homogeneously distributed stress components in the polymer type fiber composites have been shown in this study by using finite element method.

The results obtained from this study were summarized as below::

1. The developing stress concentrations at the fiber-interface and interface-matrix common surfaces showed that the increase in fiber content was inversely proportional to the reduction in stress values.

2. Fiber volume fraction range from 4.98 to 11.87 was examined. Although the generated number of elements was different in the FE modeling of fiber composite structures, the obtained results of analysis were converged to the definite values. In the examined fiber volume fractions, the numerically calculated elastic constant values changed in small degree. The distribution of all values obtained from FEM was calculated in terms of polynomials, so that all resultant values were followed the polynomial properties.

3. In the FE modeling, the thickness of the interface region was changed in proportional to the fiber diameter and then obtained resultant elastic constant remained in a stable range. The total changes for fiber-interface-matrix and fiber-matrix models were obtained as 0.046 and 0.061 GPa mutually.

4. The application of the mechanical load per node $\left(P = 0.1 \times 10^{-4}\ \mathrm{N}\right)$ gave the elastic constants 1.39 and 1.18 GPa for fiber and matrix sections of the $d = 80\ \mu$m microcomposite by Ansys code FE analysis. While the applied load affected the entire combined structure, some portions of the stress were transferred to the other sections of the composite body. Therefore, the original individual material properties of the composite material could not be measured after loading stage.

5. The maximum developing stress distribution was seen on the composite fiber section while the maximum developing y-displacement u_y was developed on the composite matrix section.

6. The generated mesh system was not symmetric in composite cylinder transverse cross sections. The developing displacement distribution u_y on the composite fiber section showed symmetric configuration in the center of the main axis $\left(P = 0.1 \times 10^{-4} N\right)$ (**Figure 28**). The developing displacement distribution u_y in the composite matrix section localized at the end portions of the matrix portion of the cylinder.

7. In the analysis, the fiber in the matrix material was moved along the y-axis under tensile loading. The fiber material was deformed by the help of stress transmission from matrix to fiber. The role of the difference in Young's modulus and Poisson's ratio of the fiber and matrix material on deformation analysis should be considered (**Figure 29**).

8. In this study, it was determined that the fiber content of fiber/interface/matrix composition was significant in the stress distribution in all PPE/PP composite models and this was confirmed by using FEA. With less fiber content (V_f%), stress concentration at the fiber-matrix interface was found to be larger.

http://dx.doi.org/10.5772/65002

9. When three layers of the composite compared, the fiber material carried higher stresses than the interface and the interface material carried higher stresses than the matrix. This was displayed as $\left(\sigma_y^{fiber} \geq \sigma_y^{interface} \geq \sigma_y^{matrix}\right)$.

10. According to our study, when high fiber content in the matrix material was present, the matrix material decreased and the stress transfer mechanism in this case was broken (**Table 2**).

11. In our analysis work, the obtained results of stress distributions were applied for all models of discontinuous fiber embedded into the matrix material. The stress distribution results obtained from discontinuous fiber were compared with continuous fiber analytical results for the commercial engineering applications (**Tables 1** and **2**).

12. In this research, the end-face effect of the fiber was considered by placing interface in the ends.

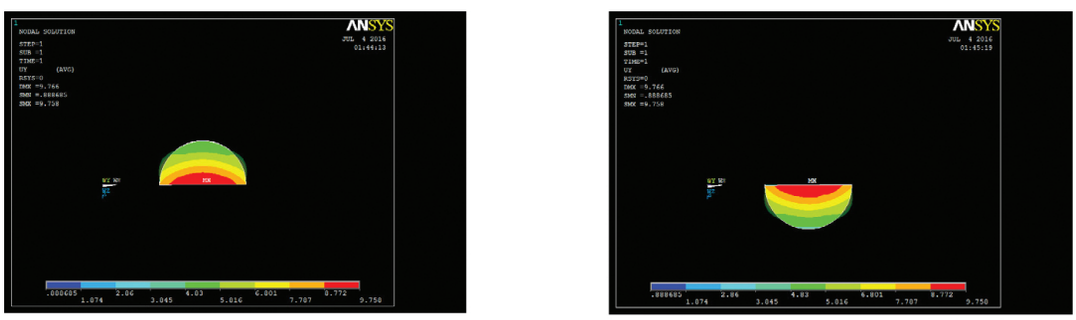

(a) (b)

Figure 28. Comparison of stress distributions $\left(\sigma_y\right)$ obtained from the cross section of the RVE FE model for mechanical load ($d = 80\ \mu$m): (a) fiber without interface volume 1, (b) fiber without interface volume 2.

(a) (b)

Figure 29. Comparison of displacement distributions (deformed/undeformed shapes) of the fiber obtained from the cross section of the RVE FE model ($d = 80\ \mu$m): (a) fiber without interface volume 1, (b) fiber without interface volume 2 (force loading $Force/Node = 0.1$ N).

Three main conclusions obtained from this research were evaluated for the values of the matrix/fiber diameters and their effect on the equivalent elastic constant.

The first conclusion was presented by the comparison curve that plotted by the "linear trendline curve" representing the average differences between two FE models. The relative percentage change of the equivalent elastic constant value E_1 in the two main models was decreased as the diameter increased proportionally (**Table 2** and **Figure 30**). Adding the interface with the small diameter fiber into the cylinder strengthens the composite structure.

The second conclusion was described in the fiber-matrix models. The diameter of the fiber increased from 40 to 55 μm in an order. As a result of this application, the equivalent elastic constant of the composite cylinder E_1 was increased from 1.054 to 1.081 GPa in proportion. The decrease in elastic modulus value E_1 was obtained from 1.063 to 1.047 GPa in a nonlinear manner for the diameter ranges from 60 to 80 μm.

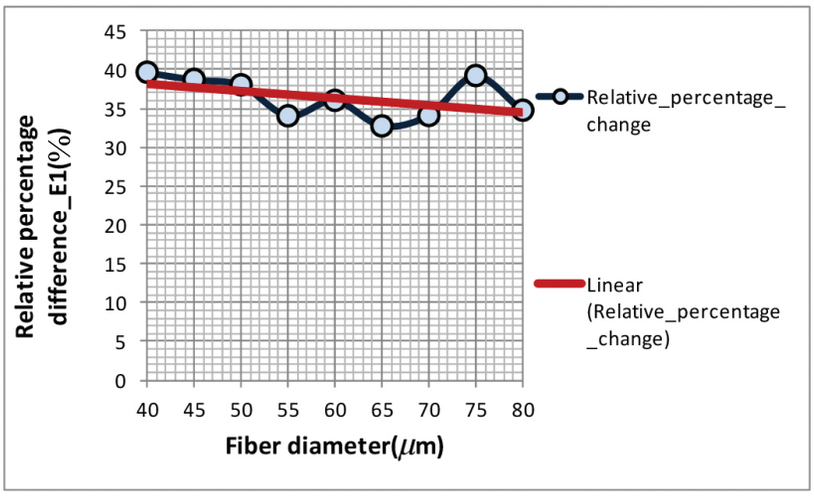

Figure 30. Comparison E_1 between fiber-matrix and fiber-interface-matrix FE models.

The third conclusion was explained for the fiber-interface-matrix model. As the diameter increased from 40 to 65 μm, the equivalent elastic constant E_1 of the microcomposite decreased from 1.472 to 1.415 GPa linearly. However, the decrease in elastic modulus value E_1 between the diameters 70 and 80 μm was obtained as 1.428 and 1.411 GPa in a nonlinear manner.

These results explained us that within the limits of 4.98–9.37% fiber volume fraction, proportionally increased interface volume caused the linearly decreasing elastic modulus value E_1. Within the same limits, the fiber-matrix microcomposite had a linearly increasing value. The interface volume worked as a brake in the composite system. The interface volume reduced the stresses passing from matrix to fiber, and this region worked as a damper in a spring-damper mechanical system. For the fiber volume, fraction ranges from 1022 to 11.87%, the interface volume caused a nonlinear decreasing in the equivalent elastic modulus values, and similarly, the fiber-matrix microcomposite had a decreasing value as nonlinear.

http://dx.doi.org/10.5772/65002

In other words, the physical meaning of the fiber matrix interaction behaviors was dependent on the interface volume. Interface volume caused a general linearity between the dimensions of the fiber, matrix, and the calculated equivalent elastic constant value (**Table 1**).

As a future work,, the effects of dimensional properties of composite models obtained in this study can be introduced into semi-empirical model (Halpin-Tsai) based on elasticity equations by curve fitting.

Acknowledgements

Thanks for the great supports of FIGES and BAP project under grant no. 06/2011-57. This study was performed in Department of Mechanical Engineering, Gazi University, Ankara, Turkey.

Nomenclature

Symbols

C_{ij}	elastic constants matrix $\left(\mathrm{N/m^2}\right)$
d	diameter of the fiber $(\mu\mathrm{m})$
$E_{1'}\left(E_1\right)_{avg}$	equivalent Young's modulus and average equivalent Young's modulus parallel to fiber direction $\left(\mathrm{N/m^2}\right)$
E_2	Young's modulus perpendicular to the fiber $\left(\mathrm{N/m^2}\right)$
$E_{f'}, E_{m'}, E_i$	Young's modulus of fiber, matrix, and interface materials $\left(\mathrm{N/m^2}\right)$
$G_{f'}, G_{m'}, G_i$	Shear modulus of fiber, matrix, and interface materials $\left(\mathrm{N/m^2}\right)$
G_{12}	in-plane shear modulus $\left(\mathrm{N/m^2}\right)$
ℓ	length of the fiber $(\mu\mathrm{m})$
L	length of the matrix $(\mu\mathrm{m})$
P	force loading (N)
S	diameter of cylindrical matrix segment $(\mu\mathrm{m})$
t_i	thickness of the interface tubular volume $(\mu\mathrm{m})$
t_{app}	loaded thickness of the composite cylinder $(\mu\mathrm{m})$
U_y	displacement type loading $(\mu\mathrm{m})$

$u_{x'}u_{y'}u_z$ displacements parallel to the x, y, z directions in an order $(\mu\mathrm{m})$

$V_{f'}V_m$ fiber and matrix volume fractions

Greek symbols

$\nu_{f'}\nu_m$ Poisson's ratio of fiber and matrix

ν_{12} major in-plane ratio

ξ reinforcing factor

σ_i stress vector $\left(\mathrm{N}/\mu\mathrm{m}^2\right)$

$\sigma_{y'}y$ -directional stress component $\left(\mathrm{N}/\mu\mathrm{m}^2\right)$

σ_2 Von Mises stress component $\left(\mathrm{N}/\mu\mathrm{m}^2\right)$

ε_i strain vector

$\theta_{x'}\theta_{y'}\theta_z$ displacements parallel to the x, y, zdirections in an order (rad).

Author details

Ezgi Günay

Address all correspondence to: ezgigunay@gazi.edu.tr

Department of Mechanical Engineering, Gazi University, Maltepe, Ankara, Turkey

References

[1] Termonia Y. Computer model for the elastic properties of short fibre and particulate filled polymers. Journal of Materials Science. 1987;22:1733–1736.

[2] Termonia Y. Theoretical study of the stress transfer in single fibre composites. Journal of Materials Science. 1987;22:504–508.

[3] Termonia Y. Fibre coating as a means to compensate for poor adhesion in fiber-reinforced materials. Journal of Materials Science. 1990;25:103–106.

[4] Termonia Y. Effect of strain rate on the mechanical properties of composites with a weak fibre/matrix interface. Journal of Materials Science. 1992;27:4878–4882.

[5] Termonia Y. Tensile strength of discontinuous fibre-reinforced composites. Journal of Materials Science. 1990;25:4644–4653.

[6] Termonia Y. Dependence of fibre critical length on modulus in single-fibre composites. Journal of Materials Science Letters. 1993;12:732–733.

[7] Sun CT, Vaidya RS. Prediction of composite properties from a representative volume element. Composites Science and Technology. 1996;56:171–179.

[8] Li VC, Kanda T, Lin Z. The influence of fiber/matrix interface properties on complementary energy and composite damage tolerance. In: Proceedings of 3rd Conference on Fracture and Strength of Solid, December 1997; Hong Kong.

[9] Kang GZ, Gao Q. Tensile properties of randomly oriented short δ-Al_2O_3 fiber reinforced aluminum alloy composites: II. Finite element analysis for stress transfer, elastic modulus and stress-strain curve. Composites Part A. 2002;33:657–667.

[10] Houshyar S, Shanks RA, Hodzic A. The effect of fiber concentration on mechanical and thermal properties of fiber-reinforced polypropylene composites. Journal of Applied Polymer Science. 2005;96:2260–2272. doi:10.1002/app.20874

[11] Hbaieb K, Wang, QX, Chia YHJ, Cotterell B. Modelling stiffness of polymer/clay nanocomposites. Polymer. 2007;48:901–909. doi:10.1016/j.polymer.2006.11.062

[12] Lee SH, Wang S, Pharr GM, Xu H. Evaluation of interphase properties in a cellulose fiber-reinforced polypropylene composite by nanoindentation and finite element analysis. Composites: Part A. 2007;38:1517–1524. doi:10.1016/j.compositesa.2007.01.007

[13] Houshyar S, Shanks RA. Hodzic A. Modelling of polypropylene fiber-matrix composites using finite element analysis. Express Polymer Letters. 2009;3(1):2–12. doi:10.3144/expresspolymett.2009.2

[14] Kim BR, Lee HK. An RVE-based micromechanical analysis of fiber-reinforced composites considering fiber size dependency. Composite Structures. 2009;90:418–427. doi: 10.1016/j.compstruct.2009.04.025.

[15] Porfiri M, Gupta N. Effect of volume fraction and wall thickness on the elastic properties of hollow particle filled composites. Composites: Part B. 2009;40:166–173. doi:10.1016/j.compositesb.2008.09.002

[16] Pan Y, Pelegri AA. Influence of matrix plasticity and residual thermal stress on interfacial debonding of a single fiber composite. Journal of Mechanics of Materials and Structures. 2010;5(1):129–142.

[17] Pal B, Haseebuddin MR. Analytical estimation of elastic properties of polypropylene fiber matrix composite by finite element analysis. Advances in Materials Physics and Chemistry. 2012;2:23–30. doi:org/10.4236/ampc.2012.21004

[18] Sockalingam S, Nilakantan G. Fiber-matrix interface characterization through the microbond test. International Journal of Aeronautical and Space Sciences. 2012;13(3): 282–295. doi:10.5139/IJASS.2012.13.3.282

[19] Qing H. A new theoretical model of the quasistatic single-fiber pullout problem: analysis of stress field. Mechanics of Materials. 2013;60:66–79. doi:org/10.1016/j.mechmat.2013.01.006

[20] Sai VS, Satyanarayana MRS, Murthy VBK, Rao GS, Prasad AS. An experimental simulation to validate FEM to predict transverse Young's modulus of FRP composites. Hindawi Publishing. Corporation Advances in Materials Science and Engineering Article. ID 648527, 1–6, 2013. doi:org/10.1155/2013/648527

[21] Unterweger C, Brüggemann O, Fürst C. Effects of different fibers on the properties of short-fiber-reinforced polypropylene composites. Composites Science and Technology. 2014;103:49–55. doi:org/10.1016/j.compscitech.2014.08.014

[22] Alfonso I, Iglesias VR, Figueroa IA. Computational potentialities of the finite elements method for the modeling and simulation of composite materials: a review. Revista Materia. 2015;20(2):293–303. doi:10.1590/S1517-707620150002.0030

[23] Chang WX, Qing H, Gao CF. A new theoretical model of the quasistatic single-fiber pull-out problem: a rate-dependent interfacial bond strength. Mechanics of Materials. 2016;94:132–141. doi:org/10.1016/j.mechmat.2015.12.001

[24] Jones RM. Mechanics of composite materials. New York: (Taylor &Francis Group) CRC Press; 1998. 538 p.

[25] Paul B. Prediction of elastic constants of multiphase materials. Transactions of the Metallurgical Society of AIME. 1960;218:36–41.

[26] Cox HL. The elasticity and strength of paper and fibrous materials. Search Results British Journal of Applied Physics. 1952;3(72):72–79.

[27] Günay E, Ece Z, Esi MA. A comparative study of fiber-matrix interactions by using micromechanical models. Mechanics of Composite Materials. 2008;44(4):505–520. doi: 10.1007/s11029-008-9027-8